Structure Formation in Strongly Correlated Coulomb Systems

M. Bonitz[1], V. Filinov[2], A. Filinov[1], V. Golubnychiy[1], P. Ludwig[1,3], H. Baumgartner[1], P.R. Levashov[2], V.E. Fortov[2], and H. Fehske[4]

[1] Institut für Theoretische Physik und Astrophysik, Christian-Albrechts-Universität zu Kiel, Leibnizstr. 15, 24098 Kiel
[2] Institute for High Energy Density, Russian Academy of Sciences, Izhorskaya 13/19, 127412 Moscow, Russia
[3] Institut für Physik, Universität Rostock, Universitätsplatz 3, 18051 Rostock
[4] Institut für Physik, Ernst-Moritz-Arndt-Universität Greifswald, Domstrasse 10a, 17489 Greifswald

Abstract. We present an overview on classical and quantum Coulomb (Wigner) crystallization phenomena caused by strong correlation effects in one-component and two-component plasmas.

1 Introduction

Coulomb systems (CS) built-up by charged particles are omnipresent in nature [1,2] - from astrophysical plasmas (interior of planets or stars [3]) to laboratory systems (gas discharges, fusion plasmas, trapped ions, plasmas in storage rings or dusty plasmas to name a few examples [4]). Due to the strength and long range of the Coulomb interaction it dominates the many-particle behavior in these systems. Despite their different form of appearance, all CS exhibit similar fundamental properties governed by the strength of the Coulomb interaction (measured by the coupling parameters Γ and r_s) and the importance of quantum effects (quantified by the degeneracy parameter χ). These parameters are determined by the ratio of characteristic energy and length scales [5–7]:

- *Length scales*: (i) $\bar{r}$ – average inter-particle distance, $\bar{r} \sim n^{-1/d}$ (n and $d = 1, 2, 3$ denote the density and dimensionality of the system, respectively). (ii) Λ – quantum-mechanical extension of the particles. For free particles we have $\Lambda = h/\sqrt{2\pi m k_B T}$ (DeBroglie wavelength), for bound particles Λ is given by the extension of the wave function. (iii) a_B – relevant Bohr radius $a_B = \frac{\epsilon}{e_a e_b}\frac{\hbar^2}{m_{ab}}$, where $m_{ab}^{-1} = m_a^{-1} + m_b^{-1}$.
- *Energy scales*: (i) $\langle K\rangle$ – mean kinetic energy, which in a classical system is given by $\langle K\rangle_{cl} = \frac{d}{2}k_B T$, whereas in a highly degenerate Fermi system $\langle K\rangle_{qm} = \frac{3}{5}E_F$ holds (E_F denotes the Fermi energy); (ii) $\langle U_c\rangle$ – mean Coulomb energy, given for free and bound particles by $\langle U_c\rangle_f = \frac{e_a e_b}{4\pi\epsilon}\frac{1}{\bar{r}}$ and $\langle U_c\rangle_B = \frac{e_a e_b}{4\pi\epsilon}\frac{1}{2a_B} \equiv E_R$, respectively.

Then the *degeneracy parameter* $\chi \equiv n\Lambda^d \sim (\Lambda/\bar{r})^d$ divides many-body systems into classical ($\chi < 1$) and quantum mechanical ones ($\chi \geq 1$).

The *Coulomb coupling parameter* is the ratio $|\langle U_c \rangle|/\langle K \rangle$. For classical systems $\Gamma \equiv |\langle U_c \rangle|/k_B T$ results, whereas for quantum systems the role of Γ is taken over by the Brueckner parameter $r_s \equiv \bar{r}/a_B \sim |\langle U_c \rangle|/E_F$.

This way the equilibrium state of a plasma containing a single charge component can be characterized, but also two-component Coulomb systems can be classified (see Sec. 5 below).

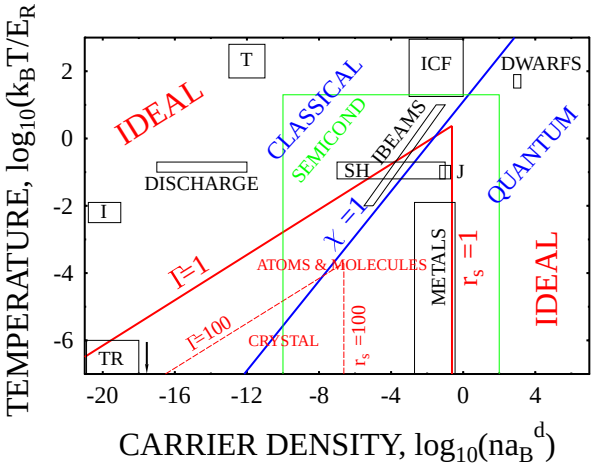

Fig. 1. Universal density–temperature plane for one-component Coulomb systems in thermodynamic equilibrium. The lines $\Gamma = 1$ and $r_s = 1$ enclose the region of strong Coulomb correlations, the lines $\Gamma = 100$ and $r_s = 100$ give an approximate boundary for Coulomb (Wigner) crystals. The line $\chi = 1$ separates classical (left) and quantum (right) systems. Abbreviations stand for CS in tokamaks (T), inertial confinement fusion (ICF), brown dwarf stars (DWARFS), Jupiter interior (J), ionosphere (I), shock wave plasmas (SH), ion beams (IBEAMS). The green box denotes the region of semiconductors (scaled with the excitonic a_B, E_R). Plasmas in traps (TR), typically realized at sub-Kelvin temperatures, are outside the figure (taken from [7].)

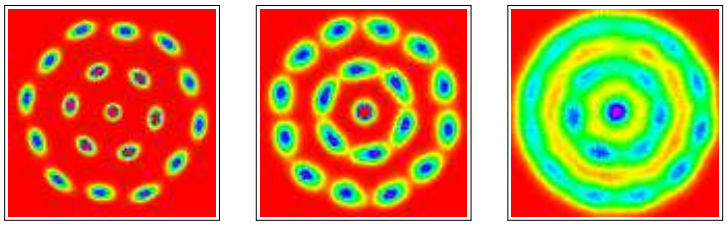

Fig. 2. 19-electron quantum Wigner "crystal" (left), radially ordered crystal (center) and mesoscopic fermionic liquid (right). From left to right quantum melting at constant temperature occurs. Dots correspond to the probability density ρ of the electrons in the 2d plane which varies between ρ_{max} (pink) and zero (red) [8].

Fig. 1 shows a qualitative phase diagram of one-component Coulomb systems in equilibrium as a function of temperature and density. Different Coulomb systems can be mapped onto each other by rescaling lengths and energies in the actual a_B and E_R (with the corresponding data for m, e, d, and ϵ). Applying this rescaling to electron-hole plasmas in semiconductors one sees that it covers a remarkably broad range of situations in laboratory and space plasmas.

The general behavior of CS is well known: In the limit of high temperature $\chi \ll 1$ and $\Gamma \ll 1$, the CS behaves as a *classical ideal gas* of free charge carriers. Similarly, in the limit of very high densities, the degeneracy becomes large, i.e. $\chi \gg 1$, and the Fermi energy exceeds the interaction energy ($r_s \ll 1$), leading to an *ideal quantum gas* of spatially extended and mutually penetrating particles. Much more interesting behavior emerges when the Coulomb energy starts to exceed the kinetic energy, i.e., $\Gamma \geq 1$ or $r_s \geq 1$. Then the charged particles become highly coordinated showing liquid-like correlations. Increasing Γ and r_s further to values of the order of 100, it is energetically favorable for the charged particles to settle in a lattice arrangement. This process was originally predicted to occur for electrons in metals by Wigner [9]. The possible existence of Wigner crystals (we will use the term *Coulomb crystal* as a synonym) in different CS will be in the focus of this overview.

The occurrence of strong Coulomb correlations is inhibited by many competing effects. The most important is bound state formation of atoms or molecules, which are neutral and thus drastically reduce the coupling strength in the system, (for a detailed analysis of Coulomb bound states see [1,2]). For this reason the realization of Wigner crystals turned out to be very difficult. It was first achieved with electrons on the surface of ultra-cold Helium droplets [10]. Here bound state formation was suppressed by the use of a *one-component* system being stabilized due to the image forces on the droplet surface. This idea was further exploited in other one-component plasma systems (non-neutral plasmas), in particular for ions [11,12] trapped in electrostatic confinement potentials (for an overview and additional references see [4]). Below, we consider examples of such non-neutral plasmas in two and three dimensions. We conclude by discussing Coulomb crystallization in *two-component* (neutral) plasmas.

2 Theoretical basis

The Hamiltonian of a one-component CS of identical particles with mass m and charge e in a confinement potential $V(r)$ is given by

$$\hat{H} = \sum_{i=1}^{N} \left[-\frac{\hbar^2}{2m}\nabla^2 + V(\mathbf{r}_i) + \frac{e^2}{\epsilon} \sum_{1 \leq j < i}^{N} \frac{1}{|\mathbf{r_i} - \mathbf{r_j}|} \right] . \tag{1}$$

Throughout this paper the confinement will be assumed to be isotropic and parabolic, i.e. $V(r) = m\omega^2 r^2/2$. The last, pair interaction term in Eq. (1) is repulsive, and the particle arrangement is stabilized by the external potential V that drives the particles towards the center ($\mathbf{r} = 0$). Depending on temperature

and density (which is controlled by the trap frequency ω) the system (1) shows a rich many-particle behavior, where in finite systems with $N < 100$ the properties strongly depend on the precise particle number. Nevertheless structural transitions such as crystallization and melting occur being reminiscent of phase transitions in real macroscopic systems. We will, therefore, use this terminology here as well, always keeping in mind the peculiarities of a finite system.

In particular, *melting* in these mesoscopic systems can be understood, in analogy to macroscopic systems, as a process of abrupt loss of spatial correlations, i.e. as an increase of relative *inter-particle distance fluctuations* u,

$$u \equiv \frac{2}{N(N-1)} \sum_{i \neq j}^{N} \sqrt{\frac{\langle r_{ij}^2 \rangle}{\langle r_{ij} \rangle^2} - 1}, \tag{2}$$

where r_{ij} is the distance between particles i and j. The average is evaluated in thermodynamic equilibrium either as a time average, e.g. in a kinetic or molecular dynamics (MD) simulation, or as an ensemble average in a (classical or quantum) Monte Carlo (MC) simulation (cf. Ref. [13]). These quantities are readily computed in any dimension, for macroscopic and small ensembles and for classical and quantum systems as well. Some representative examples will be shown below (see Fig. 5). The distance fluctuations show a drastic increase when the system goes over from localized to delocalized behavior and therefore can be taken as a suitable criterion for a melting-like transition even in small systems [14].

Let us emphasize that the *theoretical analysis* of Coulomb crystallization is very difficult. Due to the strong correlations no rigorous analytical methods exist. So one has to resort to computer simulations such as MD or MC. The problem is even more difficult in quantum systems because additionally quantum diffraction and spin effects occur. The results presented in figures 2, 4, 6, and 9 below have been obtained from first principle path integral Monte Carlo (PIMC) simulations where the most probable configuration in the canonical ensemble is computed evaluating the density operator $\hat{\rho} = Z^{-1} e^{-\hat{H}/k_B T}$ (for details see again Ref. [13]). PIMC simulations have been dramatically improved over the last 10 years, where an important impact are high-quality quantum pair potentials modelling quantum effects at small distances. Such potentials were originally derived by Kelbg and Ebeling [15,16] and continuously improved by Ebeling and co-workers (for recent reviews see [17,18], PIMC simulations of macroscopic plasmas were discussed in Refs. [19,20,13]).

3 Two-dimensional plasmas in traps

Let us first consider the motion of particles being confined to a plane of zero thickness. Practically, finite thickness effects can always be taken into account by using in Eq. (1) effective potentials (averaged over the particle wave functions in the third dimension [13]).

3.1 Crystallization in classical 2d plasmas

The classical ground state is obtained by neglecting the kinetic energy ($T \to 0$), i.e. by minimizing the total potential energy [second plus third terms in Eq. (1)]. Since $\Gamma \to \infty$ (the critical value for a macroscopic 2d plasma is 137) a Coulomb (Wigner) crystal is formed which consists of several concentric shells. The shell occupation numbers form a regular sequence like in the case of the Mendeleyev table of atoms (see, e.g., Ref. [21] and references therein). Besides the shell structure, these crystals form a triangular lattice (with hexagonal symmetry), which is the ground state of a macroscopic 2d Coulomb system, see e.g. Fig. 2. As the temperature increases, melting occurs in two steps. First a "delocalization" of particles within their shells is observed which we denote as *orientational melting* (OM). Here the radial order is still retained, see Fig. 3. Second, a substantial radial overlap of the shells occurs leading to a cross-over to a fluid-like state. This is process is called *radial melting* (RM). Remarkably, the stability of small crystals against fluctuations and finally melting varies drastically with N due to differences in the symmetry. Particular high stability against OM is observed for so-called "magic" clusters with closed shells (e.g. $N = 19$), cf. the corresponding phase boundaries of the clusters with $N = 19$ and the "non-magic" cluster $N = 20$ in Fig. 4.

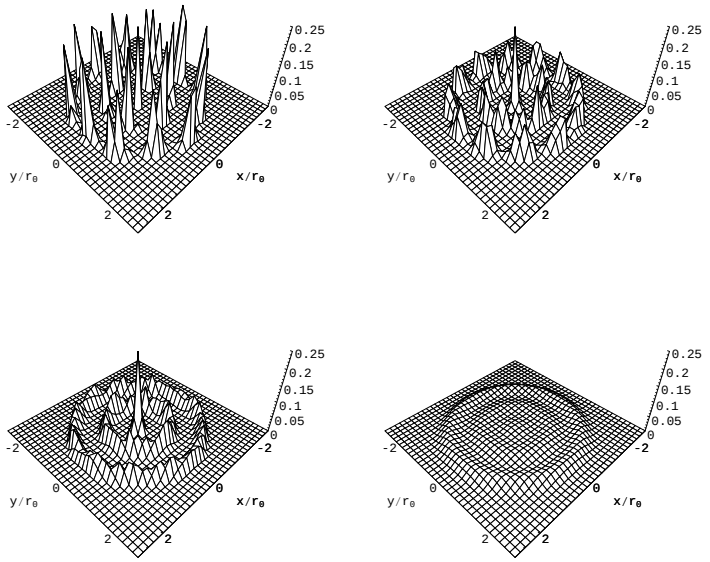

Fig. 3. Probability distribution function for a classical Coulomb cluster with $N = 19$ for $\Gamma = 300$ (top left), $\Gamma = 150$ (top right), $\Gamma = 100$ (bottom left) and $\Gamma = 10$ (bottom right). Orientational (radial) melting is observed from left to right in the top (bottom) line. r_0 is defined by $e^2/\epsilon_b r_0 = m^* \omega^2 r_0^2/2$ (taken from Ref. [22]).

3.2 Crystallization in quantum 2d plasmas

Of course the limit $\Gamma \to \infty$ is not realized in nature because with vanishing temperature or increasing density quantum effects become important. The degeneracy parameter χ will unavoidably exceed unity, what means that the coupling strength is no longer determined by Γ but by r_s. As a consequence, an increase of the density increase will lead to a decrease of the coupling (because the Fermi energy increases faster than the Coulomb energy when the system is compressed) and *quantum melting* of the Wigner crystal takes place, even at zero temperature [14]. This is visualized in Fig. 2, where the crystal (left figure) vanishes by compression in two steps. In contrast to the classical case, where melting is mainly triggered by an increasing amplitude of the thermal fluctuations of particles in their local potential wells, in the quantum case, melting is due to an increasing overlap of the wave function (see the increasing size of the dots in the center figure). As a result, the electrons become able to tunnel between neighboring lattice sites, i.e. delocalization of the particles takes place. Above a critical density of about $r_s = 50$ (in a macroscopic quantum crystal melting occurs for $r_s = 37$ [23]) the crystal vanishes.

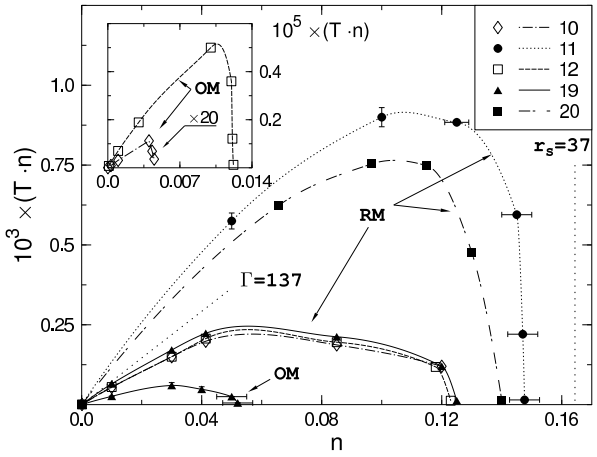

Fig. 4. Phase diagram of mesoscopic electron Wigner crystal for different particle numbers N. OM (RM) mark the boundaries of orientational (radial) melting. Here the dimensionless density n and temperature T are defined as $n = \sqrt{2}\, l_0^2/r_0^2 = (a_B^*/r_0)^{1/2} \approx r_s^{-1/2}$ and $T = k_B T/E_c$, respectively, where $l_0^2 = \hbar/(m^*\omega_0), E_c = e^2/\epsilon_b r_0$ with r_0 are given by $e^2/\epsilon_b r_0 = m^*\omega^2 r_0^2/2$ (taken from Ref. [14]).

This means, density increase, at low but finite temperature, leads to a sequence of four phase transitions (see Fig. 4): (i) A transition from a classical liquid to a classical radially only ordered (RO) crystal (e.g. for $N = 19$, this happens at $\Gamma = 330$), then (ii) to a fully ordered crystal ($\Gamma = 154$, see also Fig. 3) which (iii) transforms by quantum melting into a RO crystal at $r_s = 400$ and, finally, (iv) to a (fermionic) liquid-like state at $r_s = 64$. As a consequence

of the symmetry effects mentioned above, the "crystalline" phase is strongly particle-number dependent (cf. the different lines in Fig. 4). We would like to stress that spin effects are of minor importance with regard to the boundary of the crystalline state, but are of relevance in the liquid and gas state.

3.3 Crystals in electron bilayers

The above analysis of crystallization in two dimensions is straightforwardly extended to systems of two ore more coupled layers – from bilayers to superlattices being situated in between 2d and 3d systems. The obvious generalization of the Hamiltonian (1) consists in the replacement $\hat{H} \to \sum_a \hat{H}_a + \sum_{a \neq b} \hat{V}_{ij}^{a,b}$, where a, b label the layers. Here, as a new ingredient, the interaction $\hat{V}_{ij}^{a,b}$ between particles in different layers appears, which strongly affects the crystal structure and melting behavior [24].

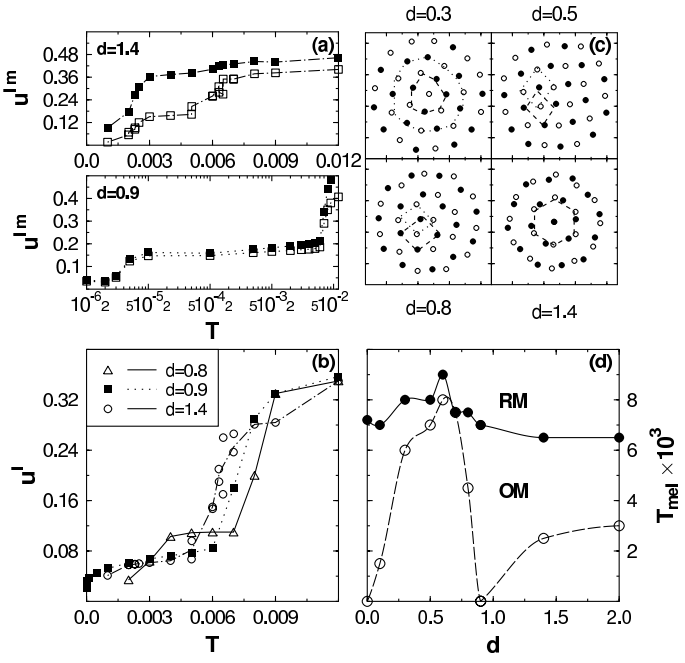

Fig. 5. Crystallization phenomena in a classical bilayer system of 2×19 particles with different interlayer distance d. Left three figures: Relative two-particle distance fluctuations u^{lm} for particles from the same layer (open symbols) and from different layers (full symbols), as well as radial fluctuations u^l (cf. Ref. [25]). Upper right panels: Snapshots of the crystal structure in the ground state. Here full and open symbols denote particles from different layers, thin lines are guides for the eye in order to underline the cluster symmetry. Lower right figure: Critical temperature of the radial (RM) and orientational (OM) melting transitions versus d [25].

Interestingly the strength of the *inter-layer correlations*, arising from $\hat{V}_{ij}^{a,b}$, can be controlled by varying the layer separation d (which acts as a new length scale of the system, in addition to the parameters discussed in the Introduction). This can be seen from Fig. 5.c, where, for large distances (e.g. $d/a_B = 1.4$), the symmetry in each layer is the same as in a single-layer system with 19 particles (cf. Fig. 2). With decreasing d the hexagonal symmetry is lost in favor of square and rhombic symmetries until, at small layer separations, the hexagonal symmetry is restored – but now the arrangement is the same as in a single layer containing 38 electrons. We note the non-monotonic change of the orientational and radial melting temperature with d (see Fig. 5.d [24]). Around $d/a_B = 0.9$ the barrier for inter-shell rotations vanishes (i.e., the two shells in each layer rotate freely) which can be traced back to the emerging 3d behavior at this distance: The particles in the two layers are coupled as equally strong as inside each layer, which can also be seen in the identical intra-layer and inter-layer distance fluctuations depicted in Fig. 5.b.

3.4 Excitonic crystal in electron-hole bilayers

Even more interesting is the case of two layers containing negative (electrons) and positive (holes) charges, respectively. Compared to the uniformly charged bilayer system new physical phenomena are observed when the distance d between the layers is reduced: The system goes over from two decoupled Coulomb layers to an effective single layer of particle pairs with *dipole-dipole interaction* instead of the Coulomb repulsion. At the same time, two fermions (an electron

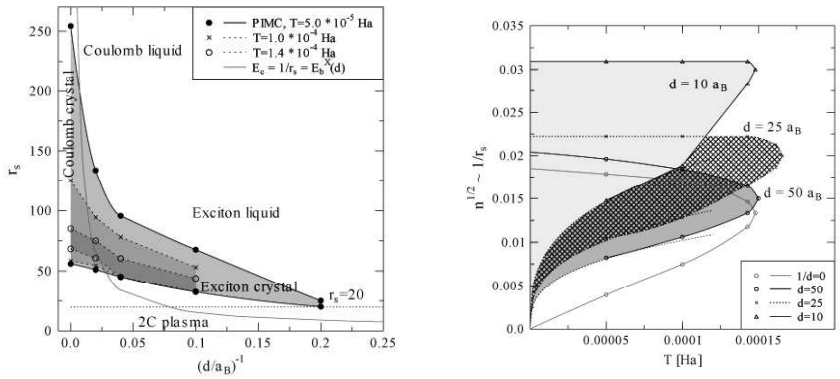

Fig. 6. Phase diagram of a symmetric ($m_e = m_h$) mesoscopic electron-hole bilayer crystal for $N_e = N_h = 16$ at fixed values of temperature (left panel). The grey line gives the boundary between plasma and excitons. Right Fig. shows the phase boundary of the crystal for fixed values of d. Results are taken from Ref. [27].

and a hole) form a bound state (*exciton*) which, to some extend, behaves as

a (composite) boson. These electron-hole bilayers also support crystallization [26,27]. In addition to the Coulomb crystals considered above (i.e., crystals of electrons and holes, respectively, in each layer at large d), one observes, at small d, crystallization of excitons. The phase diagram of this model is shown in Fig. 6. Obviously, the interlayer attraction stabilizes the crystal: The critical value of r_s is reduced to about 20 from the single layer limit of about 50 (see Fig. 4). No crystal is observed if d becomes smaller than $5a_B$, due to the large extension of the wave function in the layers [28].

Another problem of current interest regards the fluid excitonic phase. Here, our PIMC simulations give evidence that in these systems Bose condensation of excitons should be possible (note that due to their parallel orientation these "indirect" excitons repel each other and cannot form bi-excitons). From the behavior of the exchange permutation cycles [30], we find a finite Bose condensate fraction [29]. Further, a significant reduction of the moment of inertia is found which might indicate [30] a finite superfluid fraction of excitons [29].

4 Three-dimensional plasmas in traps

Coulomb crystallization in a spherical three-dimensional geometry was first observed for ultra-cold ions in Penning or Paul traps [11,12]. A second candidate are ions created by ionization of cooled trapped atoms. Recent simulations [31] show that the expanding ions might crystallize if they are properly laser cooled during the expansion. Finally, so-called "Coulomb balls" have been observed in dusty plasmas [32]. Their theoretical description is again based on a tree-dimensional version of the Hamiltonian (1) (for an overview on earlier theoretical results and simulations see [4]). In this case, for an adequate modeling of the plasma properties, the screening of the interaction has to be accounted for. The simplest approximation is to use an isotropic Debye/Yukawa potential $V(r) = e^2 \frac{e^{-\kappa r}}{r}$ instead of the Coulomb potential. Such an interaction, together with an isotropic harmonic confinement is, in fact, capable to describe the dusty plasma measurements [35]: Three-dimensional concentric shells, see Fig. 7, with shell populations N_s being sensitive to the screening strength κ. The N_s cannot be explained by using a pure Coulomb interaction. As in the 2d case closed shell configurations and a "Mendeleyev table" exist (see, e.g., Ref. [33–35]). The dependence of the crystal stability on the number of particles can be seen from their melting temperatures. For example, the closure of the first spherical shell occurs st $N = 12$, which gives rise to a particularly high crystal stability (high melting temperature), cf. Fig. 7.b. Nevertheless, many aspects of three-dimensional Coulomb crystals are still unsettled. In particular, it remains to explore the properties of 3d quantum crystals.

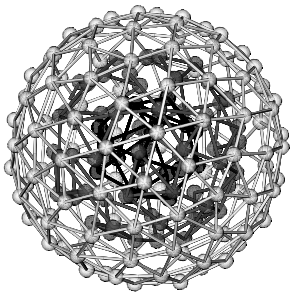

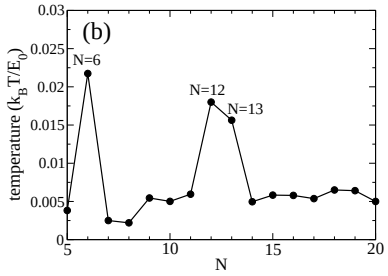

κ	N_1	N_2	N_3	N_4
0	1	18	56	115
0.2	1	18	57	114
0.3	2	20	57	111
0.4	2	20	58	110
0.5	2	21	58	109
0.6	2	21	60	107
1.0	4	24	60	102
Exp	2	21	60	107

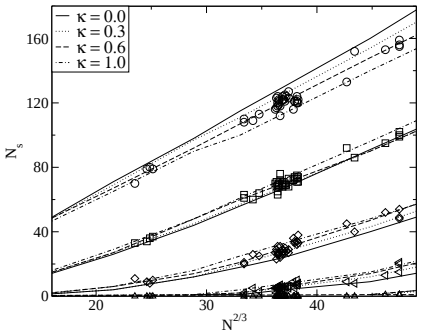

Fig. 7. Three–dimensional Coulomb crystal ("Coulomb ball"). Upper left figure shows the shell arrangement for $N = 190$, different colors denote particles on different shells (lines are a guide to the eye), lower right figure the number of particles N_s on the shells for different N and different values of κ. Upper right Fig. contains the melting temperature versus particle number. Table contains experimental (last line) and theoretical shell configurations of the Coulomb ball $N = 190$. $N_1 \ldots N_4$ denote the particle numbers on the i-th shell beginning in the center. κ is given in units of r_0^{-1} defined by $m\omega^2 r_0^2 = e^2/r_0$, temperature is in units of $E_0 = e^2/r_0$. From Refs. [35,36].

5 Coulomb crystals in macroscopic two-component plasmas

As mentioned in the Introduction, crystallization in two-component (neutral) plasmas is strongly inhibited by formation of neutral bound states. Crystal formation is nevertheless possible. One way is the formation of a crystal of neutral

particles. Due to the reduced interaction energy, however, a strongly reduced temperature is required. An example is hydrogen, where the ground state at low pressure is a molecular solid [37] and metallization is observed around 1 Mbar [38]. A similar scenario was demonstrated above in Sec. 3.4 for the case of indirect excitons which also form a crystal of neutral particles.

A second possibility is the formation of a Coulomb crystal of the heavy charge component alone. Examples are conventional metals, and similar behavior is predicted for White Dwarf stars [3] and the crust of neutron stars. In fact, also the dusty plasmas mentioned above form a Coulomb crystal in the presence of a neutralizing background. To understand the mechanisms, let us consider the characteristic parameters of a two-component plasma which generalize those of the one-component plasma discussed in the Introduction. In thermodynamic equilibrium, the "asymmetry" of the plasma is characterized by the charge and mass ratios of the heavy ("h") and light ("e") components, $Z = q_h/q_e$, $M = m_h/m_e$ and, under stationary non-equilibrium conditions, by the temperature ratio $\Theta = T_e/T_i$. In addition, now there exist coupling and degeneracy parameters for each component, Γ_e,Γ_h, r_{se}, r_{sh}, χ_e and χ_h.

The just mentioned Coulomb crystals of heavy particles occur in a strongly asymmetric neutral plasma with $Z \gg 1$ or/and $M \gg 1$ or/and $\Theta \gg 1$. Since $\Gamma_h/\Gamma_e = Z^2\Theta$, it is possible to realize situations where simultaneously strong coupling of the heavy particles but weak coupling of the light particles takes is observed. Also, there is a broad parameter range where the heavy particles are classical and the light particles are degenerate because $\chi_e/\chi_h = Z(M/\Theta)^{3/2}$. The conditions required for such a Coulomb (Wigner) crystal of heavy particles to exist in the presence of light ones (electrons) are simply that no bound states can form: Either the temperature should exceed the binding energy, or the density should be larger than the Mott density. The latter condition roughly corresponds to the situation that two neighboring electrons come closer than the size of an atom, $r_{se} < 1.2$, i.e., bound electrons can tunnel from one atom to another – a situation described in the left panel of Fig. 8. This has to be combined with the requirement of strong coupling coupling of the heavy particles, $\Gamma_h > 175$, or $r_{sh} > 100$ (in 3d). Physically this means that a crystal of heavy particles coexists within a fully delocalized gas of light ones. Both conditions can be fulfilled simultaneously for a sufficiently large charge ratio Z (as in a classical dusty plasma) or a (large) mass ratio $M > M_{cr} \approx 83$ [39,40], which allows us to predict other candidates of Coulomb crystals including crystals of protons [41], α–particles, and holes in semiconductors [39,42,43].

The numerical verification of this prediction is a challenging task which was addressed by PIMC simulations. Selected results are shown in Fig. 9. There one clearly sees continuously increased hole localization when the mass ratio is increased from $M = 12$ to 400. A hole crystal emerges between $M = 50$ and $M = 100$, in good agreement with analytical predictions [39,42]. Experimental verification of proton or $\alpha-$particle crystals seems feasible in laser or ion beam compression experiments. Also, the observation of hole crystals in semiconduc-

tors appears to be possible. Materials with sufficiently flat valence bands have already been investigated [45].

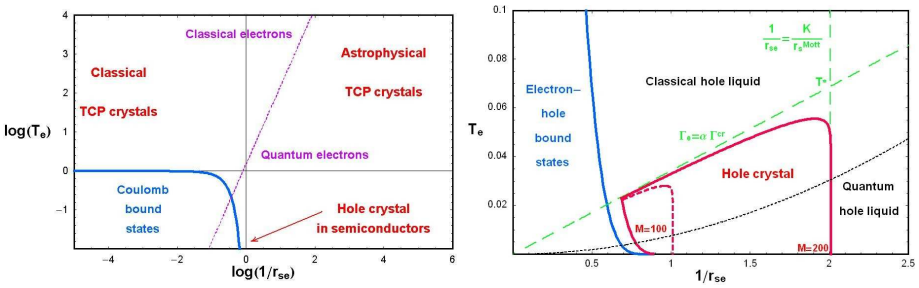

Fig. 8. Phase diagram of a Coulomb crystal of heavy particles in a macroscopic two-component (neutral) plasma. Left figure yields a qualitative picture on a larger scale. $T_e = \frac{3}{2}k_BT/E_R$ and $r_{se} = \bar{r}_e/a_B$. Taken from Refs. [39,42].

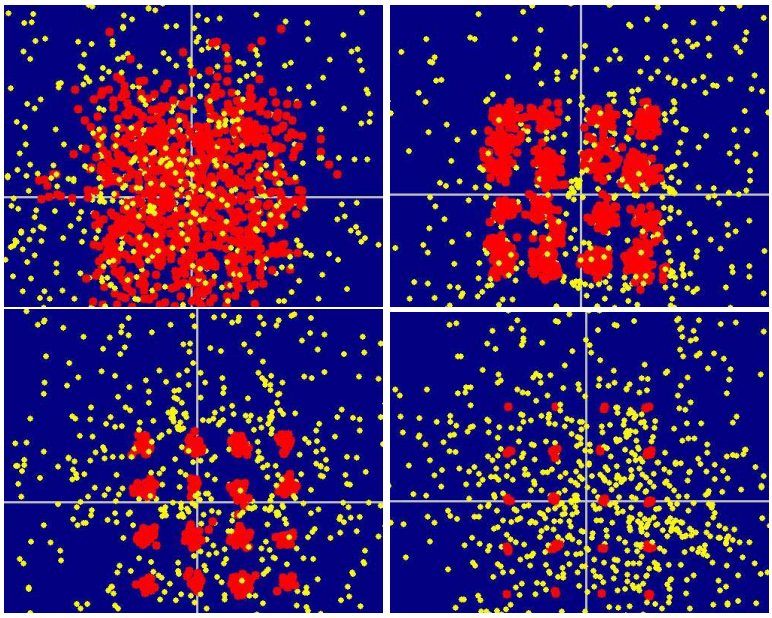

Fig. 9. Snapshots of a Coulomb crystal of heavy particles (red clouds) embedded into a Fermi gas of electrons (yellow) in a macroscopic two-component (neutral) plasma for mass ratio $M = 12$ (top left), $M = 50$ (top right), $M = 100$ (bottom left) , $M = 400$ (bottom right) [44]. The density corresponds to $r_{se} = 0.64$, the temperature is $T_e = T_h = 0.06E_R$.

6 Conclusion

We have studied structure formation in charged particle systems by unbiased numerical methods. Collective crystal-like particle arrangements have been proven to occur in finite (closed) systems. Coulomb crystals represent the energetically favorable (i.e., stable) state of the plasma in a certain density interval and at sufficiently low temperature, whereby the Coulomb coupling has to be about two orders of magnitude larger than the kinetic energy. In this report we have only considered the equilibrium properties of these finite Coulomb systems. Future research should address, e.g., the eigenmode spectrum of such clusters being directly related to their transport properties. In any case, it remains an open task, to develop a rigorous analytical theory for strongly correlated Coulomb systems in both equilibrium and non-equilibrium stituations. Further, we have discussed Coulomb crystals in macroscopic two-component neutral plasmas. The conditions for their existence are essentially a sufficiently large charge and/or mass asymmetry between the components.

Acknowledgements

It is our great pleasure to devote this overview to Werner Ebeling on the occasion of his 70th birthday. He has always been very interested in and supportive of all activities in this broad field. This work has been supported by the Deutsche Forschungsgemeinschaft via SFB-TR 24.

References

1. W. Ebeling, W.D. Kraeft, and D. Kremp, *Theory of Bound States and Ionization Equilibrium in Plasmas and Solids*, Akademie-Verlag Berlin 1976.
2. W.D. Kraeft, D. Kremp, W. Ebeling, and G. Röpke, *Quantum Statistics of Charged Particle Systems*, Akademie-Verlag Berlin 1986.
3. For details, see e.g., L. Segretain, Astron. Astrophys. **310**, 485 (1996)
4. D.H.E. Dubin and T.M. O'Neill, Rev. Mod. Phys. **71**, 87 (1999).
5. M. Bonitz, *Quantum Kinetic Theory*, Teubner, Stuttgart/Leipzig 1998.
6. M. Bonitz, Physik Journal July/August 2002, pp. 69-75.
7. M. Bonitz, D. Semkat, A. Filinov, V. Golubnychyi, D. Kremp, D.O. Gericke, M.S. Murillo, V. Filinov, W. Hoyer, and S.W. Koch, J. Phys. A: Math. Gen. **36**, 5921 (2003).
8. An illustration of these results is given in Phys. Rev. Focus, April (2001), http://focus.aps.org/story/v7/st18.
9. E. Wigner, Physical Review **46**, 1002 (1934).
10. C.C. Grimes, and G. Adams, Phys. Rev. Lett. **42**, 795 (1979).
11. D.J. Wineland, J.C. Bergquist, W.M. Itano, J.J. Bollinger, and C.H. Manney, Phys. Rev. Lett. **59**, 2935 (1987).
12. W.M. Itano et al. Science **297**, 686 (1998).
13. A. Filinov, and M. Bonitz, Chapter 4 in *Introduction to Computational Methods for Many-Body Systems*, M. Bonitz, and D. Semkat (eds.), Rinton Press, Princeton 2006

14. A. Filinov, M. Bonitz and Yu.E. Lozovik, Phys. Rev. Lett. **86**, 3851 (2001).
15. G. Kelbg, Ann. Physik, **12**, 219 (1963); **13**, 354; **14**, 394 (1964).
16. W. Ebeling, H.J. Hoffmann, and G. Kelbg, Contr. Plasma Phys. **7**, 233 (1967); K. Rohde, G. Kelbg, and W. Ebeling, Ann. Phys. **22**, 1 (1968); H. Wagenknecht, W. Ebeling, and A. Förster, Contrib. Plasma Phys. **41**, 15 (2001) and references therein.
17. A. Filinov, V. Golubnychiy, M. Bonitz, W. Ebeling, and J.W. Dufty, Phys. Rev. E **70**, 046411 (2004).
18. W. Ebeling, A. Filinov, M. Bonitz, V. Filinov, and T. Pohl, J. Phys. A: Math. Gen. **39**, 4309 (2006).
19. V.S. Filinov, M. Bonitz, W. Ebeling, and V.E. Fortov, Plasma Phys. Contr. Fusion **43**, 743 (2001).
20. S.A. Trigger, W. Ebeling, V.S. Filinov, V.E. Fortov, M. Bonitz, JETP **96**, 465 (2003).
21. V.M. Bedanov, and F.M. Peeters, Phys. Rev. B **49**, 2667 (1994).
22. V. Golubnychyi, PhD thesis, Kiel University 2004.
23. B. Tanatar, and D.M. Ceperley, Phys. Rev. B **39**, 5005 (1989)
24. For a detailed analysis of bilayers and reentrent melting, see I.V. Schweigert, V.A. Schweigert, and F.M. Peeters, Phys. Rev. Lett. **82**, 5293 (1999) and references therein.
25. A. Filinov, M. Bonitz, and Yu.E. Lozovik, Contrib. Plasma Phys. **41**, 357 (2001).
26. A. Filinov, M. Bonitz, and Yu.E. Lozovik, J. Phys. A: Math. Gen. 36, 5899 (2003).
27. A.V. Filinov, P. Ludwig, V. Golubnychyi, M. Bonitz, and Yu.E. Lozovik, phys. stat. sol. (c) 0, No. 5, 1518-1522 (2003).
28. Quantum macroscopic e-h bilayers have also been invesitaged in: S. De Palo, F. Rapisarda, and G. Senatore, Phys. Rev. Lett. **88**, 206401 (2002).
29. A.V. Filinov, P. Ludwig, M. Bonitz, and Yu.E. Lozovik, phys. stat. sol. (2006).
30. D.M. Ceperley, Rev. Mod. Phys. **67**, 279 (1995).
31. T. Pohl, T. Pattard, and J.M. Rost, Phys. Rev. Lett. **92**, 155003 (2004).
32. O. Arp, D. Block, A. Piel, and A. Melzer, Phys. Rev. Lett. **93**, 165004 (2004).
33. K. Tsuruta, and S. Ichimaru, Phys. Rev. A **48**, 1339 (1993).
34. P. Ludwig, S. Kosse, and M. Bonitz, Phys. Rev. E **71**, 046403 (2005).
35. M. Bonitz, D. Block, O. Arp, V. Golubnychiy, H. Baumgartner, P. Ludwig, A. Piel, and A. Filinov, Phys. Rev. Lett. **96**, 075001 (2006).
36. V. Golubnychiy, H. Baumgartner, M. Bonitz, A. Filinov, and H. Fehske, J. Phys. A: Math. Gen. **39**, 4527 (2006).
37. For an overview, see H.-K. Mao, and R.J. Hemley, Rev. Mod. Phys. **66**, 671 (1994)
38. S.T. Weir, A.C. Mitchell, and W.J. Nellis, Phys. Rev. Lett. **76**, 1860 (19996)
39. M. Bonitz, V.S. Filinov, V.E. Fortov. P.R. Levashov, and H. Fehske, Phys. Rev. Lett. **95**, 235006 (2005).
40. This is close to the estimate of 100 for CuCl given by A.A. Abrikosov, J. Less-Comm. Metals **62**, 451 (1978).
41. V.S. Filinov, M. Bonitz, and V.E. Fortov, JETP Letters **72**, 245 (2000).
42. M. Bonitz, V.S. Filinov, V.E. Fortov. P.R. Levashov, and H. Fehske, J. Phys. A: Math. Gen. **39**, 4717 (2006).
43. B.I. Halperin, and T.M. Rice, Rev. Mod. Phys. **40**, 755 (1968)
44. An illustration of these results is given in Phys. Rev. Focus, December 2 2005, http://focus.aps.org/story/v16/st17.
45. B. Bucher, P. Steiner, and P. Wachter, Phys. Rev. Lett. **67**, 2717 (1991); P. Wachter, B. Bucher, and J. Malar, Phys. Rev. B **69**, 0945021 (2004).